Journal of Materials Chemistry A

Accepted Manuscript

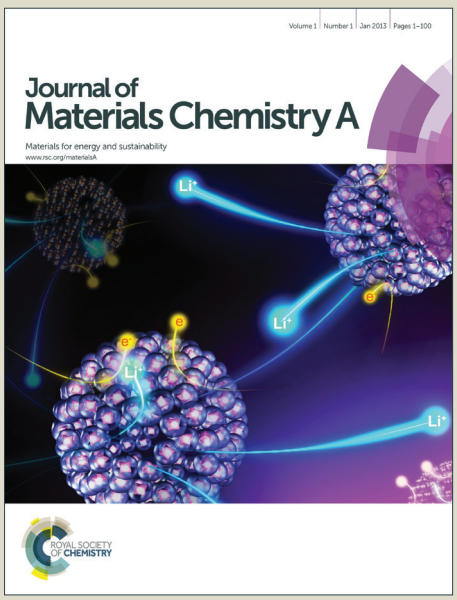

ROYAL SOCIETY OF CHEMISTRY

www.rsc.org/materialsA

Journal of
Materials Chemistry A

RSCPublishing

PAPER

Flexible, sandwich-like Ag-nanowire/PEDOT:PSS-nanopillar/MnO_2 high performance supercapacitor

Cite this: DOI: 10.1039/xoxxoooooox

Zenan Yu, Chao Li, Danielle Abbitt, and Jayan Thomas*

Received ooth March 2014,
Accepted ooth xx 2014

DOI: 10.1039/xoxxoooooox

www.rsc.org/

We demonstrate the design and fabrication of a Ag/PEDOT:PSS/MnO_2 layer by layer structure for high performance flexible supercapacitors (SCs). This is a unique design combining Ag-nanowires and PEDOT:PSS-nanopillars as current collector in SCs. In this sandwich-like structure, electrons can be easily transferred through a networked structure of Ag-nanowires to PEDOT:PSS-nanopillars and finally to the MnO_2 layer and vice versa. This scheme provides excellent specific capacitances of 862 F g^{-1} (based on MnO_2) at a current density of 2.5 A g^{-1} and robust long-term cycling stability. Moreover, SCs fabricated based on this structure exhibit exceptional flexibility and bendability (less than 2% loss in specific capacitance even after 100 bends) and high energy and power densities. All wet processing method of fabrication along with superior performance make these SCs very attractive for the next generation flexible energy storage systems.

1. Introduction

The limited availability and adverse environmental effects of many fossil fuels used today have expedited the development of various renewable energy sources such as solar, wind, and hydro power. In order to better utilize these resources, an efficient energy storage system is essential. Supercapacitors (SCs), also called electrochemical capacitors, have been considered as one of the most attractive storage systems due to their high power and energy densities. Compared to other storage systems like batteries, SCs have faster charge/discharge rate, higher power density, and longer lifetime.[1, 2] Due to these advantages, SCs have been widely employed in the emergency doors of Airbus A380, power back-up systems, public transportation, and medical devices, etc.[1, 3] To date, various transition metal oxides have been extensively studied as possible electrode materials for SCs, including RuO_2,[4] NiO,[5] CoO_x,[6] and MnO_2.[7-9] Among them, RuO_2 produces the highest specific capacitance but at a high cost and significant environmental footprint. As an alternative, MnO_2 stands out as the most promising material attributed to its remarkable features such as high specific capacitance, low cost and environment friendliness.[10-13] However, the major bottleneck of MnO_2 is its low electrical conductivity (10^{-5}-10^{-6} S cm^{-1}).[14] To address this problem, several strategies have been proposed, including depositing MnO_2 onto highly conductive nanostructures such as metal oxide nanowires, [15-18] carbon nanotubes,[19-22] carbon textile,[23-25] etc. But there have been only a few studies on depositing MnO_2 onto nanostructured conducting polymer.

Recently, Lee *et al.* have proposed MnO_2/ poly(3,4-ethylenedioxythiophene) coaxial nanowires for SC electrodes,[26, 27] but the high aspect ratio of these nanowires usually leads to the collapse of nanowires into each other, resulting in the decrease of surface area, reduction of deposited active materials and limited accessibility of electrolyte. Moreover, the nanostructure is constructed using sacrificial templates which need to be removed by reacting with dangerous chemical reagents. Therefore, constructing a highly ordered conducting polymer structure with an environment-friendly approach is critical and urgent. Recently, a Spin-on Nanoprinting (SNAP) technique is developed by our group to easily and quickly print highly ordered polymer structure using spin-coating.[28-31] However, it is difficult to print conducting polymer like PEDOT using SNAP technique because of its poor solubility. In this case, a poly(styrenesulfonate) polymer is introduced into PEDOT oligomers and forms poly(3,4-ethylenedioxythiophene):poly(styrenesulfonate) (PEDOT:PSS) which allows spin-coating of thin and conductive films. Even though the introduction of PSS into PEDOT brings an enhanced solubility, a reduced electrical conductivity is also introduced due to PSS.[32] Herein, silver nanowires (Ag-NWs) are incorporated into PEDOT:PSS nanostructure in order to enhance the electrical conductivity. The electrical conductivity of PEDOT:PSS thin film after introducing Ag-NWs is 10^3-10^4 S cm^{-1}. It is comparable to other thin film current collectors

such as PEDOT (10^2-10^3 S cm^{-1}),[33, 34] Indium Tin Oxide (ITO,

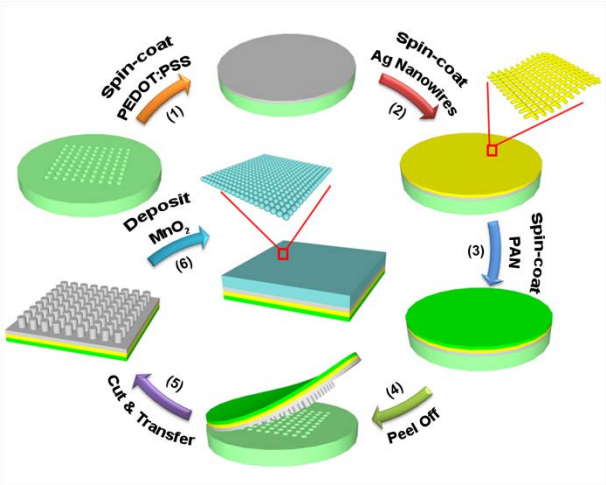

Fig. 1 Schematic illustration showing the development of sandwich-like Ag-NW/PEDOT:PSS-NP/MnO_2 structure of electrode.

10^2-10^4 S cm^{-1}),[35] CNT (10^2-10^3 S cm^{-1}),[36] Nickel (Ni, 10^4-10^5 S cm^{-1}), etc. Nanostructured PEDOT:PSS layer is also indispensable in this combined PEDOT:PSS/Ag-NW current collector due to two major reasons: (1) printed nanostructured PEDOT:PSS will provide much more surface area for depositing MnO_2 and (2) MnO_2 cannot be directly deposited onto Ag NWs because of its poor adhesion on the surface. This is based on our experimental observation.

Here, we present the design and development of novel sandwich-like Ag-nanowire/PEDOT:PSS-nanopillar/MnO_2 electrodes and their improved supercapacitor device performance. The bottom layer constitutes a networked Ag-nanowire (Ag-NW) structure. A highly ordered PEDOT:PSS-NP structure serves as the middle layer and MnO_2 functions as the third layer of the electrode. Using Ag-NW has the following advantages: First, Ag-NW is highly conductive which can boost the electrical conductivity of the electrode significantly.[37] Electrons can be transferred easily through this networked structure of Ag-NW like the transportation of vehicles in a highway. Moreover, during charging process, these moving electrons can be easily acquired by MnO_2 layer through the PEDOT:PSS-NPs where each NP acts like an exit of the highway to evacuate electrons; while in discharging process, electrons can be absorbed from MnO_2 layer by PEDOT:PSS-NPs readily and enter the Ag-NW highway immediately. Second, both MnO_2 and PEDOT:PSS suffer from mechanical instability due to the collapse of structure. Hence, by adding a Ag-NW layer can considerably enhance the mechanical stability (flexibility) of the electrode due to its networked structure which can endure bending stress.

2. Experimental

2.1 Preparation of electrodes.

Appropriate amount of PEDOT:PSS was spin-coated uniformly onto a nanoholes structure (mold) and heated at 150 °C for 15 minutes. Ag-NW solution purchased from Blue Nano (SLV-NW-35 Silver Nanowires) was then spin-coated onto the PEDOT:PSS layer and heated at 100 °C for 1 minute. A polyacrylonitrile (PAN) solution was spin-coated on top and served as a tape to peel off the Ag-NW/PEDOT:PSS composite. The PAN solution was prepared by dissolving 8wt% of high molecular weight (Mw 150,000) PAN in dimethyl formamide (DMF). MnO_2 was deposited onto the composite using an anodic electrodeposition method at a constant current of 0.5 mA cm^{-2} for 3 - 48 mins. A two-electrode configuration is used in this electrodeposition process including Ag-NW/PEDOT:PSS composite as positive electrode and a platinum sheet as negative electrode. 0.1M manganese acetate ($MnAc_2$) was used as electrolyte for electrodeposition. The final composites of Ag-NW/PEDOT:PSS/MnO_2 were washed by DI water for three times.

2.2 Fabrication of SCs.

The SCs were assembled by two identical pieces of Ag/PEDOT:PSS/MnO_2 electrodes with a porous separator (Celgard 3501, NC) sandwiched in between. The separator was pre-dipped into a 0.1M Na_2SO_4 electrolyte so that each side of the separator was fully coated with electrolyte. Two copper tapes were placed in between each electrode and separator (adhesive side towards separator) separately so as to connect to the outside circuit. Finally, a scotch tape was used to seal the whole device and only the two copper tapes were exposed outside.

2.3 Characterization.

Morphologies were characterized using scanning electron microscopy (SEM, ZEISS ULTRA 55) and atomic force microscopy (AFM, Dimension 3100 Combination SPM). Chemical compositions were analyzed by X-ray photoelectron spectroscopy (XPS, PHI 5400). To study the electrochemical properties of electrodes, a three-electrode configuration consisting of a working electrode (electrode prepared base on the materials as-synthesized), a platinum counter electrode and a saturated calomel electrode (SCE) as reference electrode was used. Cyclic voltammetry (CV) and galvanostatic charge/discharge (GCD) were performed on an electrochemical workstation (Bio-Logic, SP-150) using this three-electrode system in 0.1M Na_2SO_4. CV was carried out at different scan rates; 5, 20, 50, and 100 mV s^{-1}. GCD was measured at 2.5, 5, 12, and 25 A g^{-1}. The characterization experiments of the devices were conducted by a two-electrode system by CV and GCD with a voltage range of 0 – 0.8 V.

3. Results and discussion

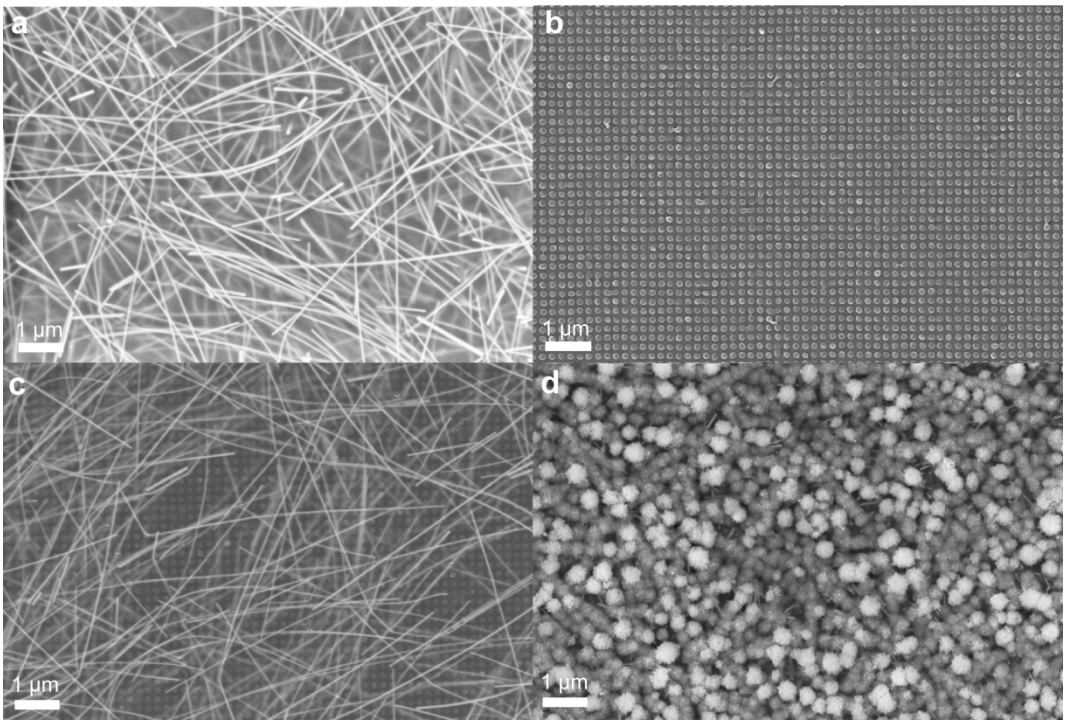

Fig. 2 SEM images of (a) pure Ag-NW layer, (b) pure PEDOT:PSS nanostructured layer, (c) Ag-NW layer beneath PEDOT:PSS nanostructured layer, and (d) Ag-NW/PEDOT:PSS-NP/MnO_2 composites.

The steps involved in the fabrication of SC electrode are presented in Fig. 1. First, a thin layer of PEDOT:PSS was spin-coated onto a silicon nanohole mold. Another layer of current collector material (Ag-NW) was then spin-coated onto the PEDOT:PSS layer. In order to remove these two layers, an additional layer of insulating polyacrylonitrile (PAN) was spin-coated onto the composite as an adhesive layer to peel off all the underlying layers from the mold. Finally, a thin layer of MnO_2 was deposited onto the PEDOT:PSS layer using electro-deposition method. Scanning electron microscope (SEM) image shown in Fig. 2a clearly shows Ag-NW layer, with Ag-NWs having an average diameter of ~35 nm and length of ~15 μm. Highly ordered PEDOT:PSS-NP structures without Ag-NW is presented in Fig. 2b and Fig. S1 (Electronic Supplementary Information, ESI), revealing that these NPs have diameter of ~130 nm and center-to-center distance of ~200 nm. PEDOT:PSS-NP with a bottom layer of Ag-NW was shown in Fig. 2c, demonstrating the networked structure of Ag-NW layer underneath PEDOT:PSS nanostructured layer. The height of NP (~30 nm) is determined by atomic force microscope (AFM) and is shown in Fig. S2 (ESI). Moreover, Ag-NW cannot be found in this AFM image, implying that the Ag-NW layer was completely covered by overlying PEDOT:PSS layer. The third MnO_2 layer is shown in Fig. 2d, indicating PEDOT:PSS-NPs were covered by MnO_2 layer so that MnO_2 can easily acquire electrons from nanopillars. A cross-sectional SEM image of Ag-NW/PEDOT:PSS-NP/MnO_2 composites is also provided in ESI Fig. S3 which further confirms the combined current collector of Ag-NW/PEDOT:PSS-NP is fully covered by MnO_2 layer.

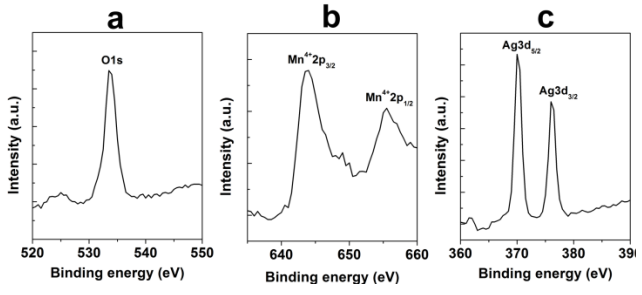

Fig. 3 XPS spectra of (a) O 1s (b) Mn 2p (c) Ag 3d for the composites.

The chemical composition of this layer by layer structure was examined by X-ray photoelectron spectroscopy (XPS). An O 1s spectrum (533.5 eV) is presented in Fig. 3a. The appearance of two peaks centered at 643.5 eV and 655.5 eV can be assigned to Mn $2p_{3/2}$ and Mn $2p_{1/2}$ (Fig. 3b), respectively, indicating Mn^{4+} was the main component from electrodeposition.[38] XPS spectrum also reveals the presence of Ag at 376 eV and 370 eV which correspond to Ag $3d_{5/2}$ and Ag $3d_{3/2}$, respectively (Fig. 3c).[39]

To evaluate the electrochemical performance of Ag-NW/PEDOT:PSS-NP/MnO_2, a three-electrode configuration in 0.1M Na_2SO_4 electrolyte was used. For comparison of performance, we used, pure Ag-NW, pure PEDOT:PSS-NP, and Ag-NW/PEDOT:PSS-NP (ESI, Fig. S4 and S5). CV curve of Ag-NW/PEDOT:PSS-NP/MnO_2 (Fig. 4a) shows much higher current density than that of Ag-NW/PEDOT:PSS-NP, indicating that MnO_2 boost the capacitive behavior

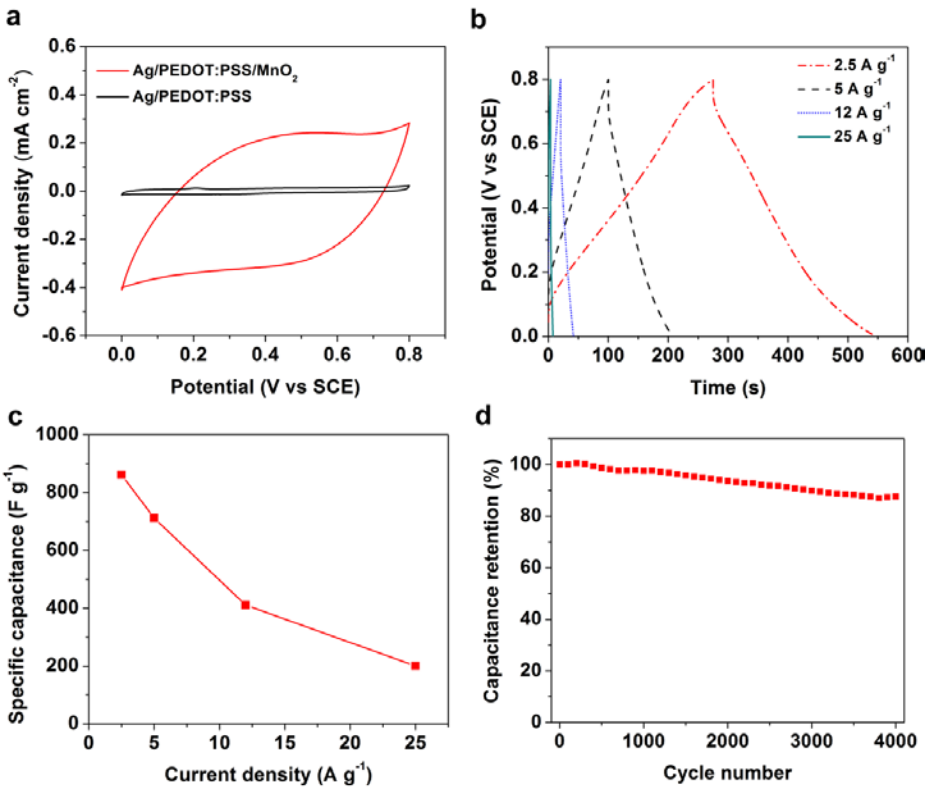

Fig. 4 (a) CV curves of Ag-NW/PEDOT:PSS-NP and Ag-NW/PEDOT:PSS-NP/MnO_2 at a scan rate of 20 mV s^{-1}. (b) GCD curves of Ag-NW/PEDOT:PSS-NP/MnO_2 at different current densities (2.5-25 A g^{-1}). (c) Specific capacitances of Ag-NW/PEDOT:PSS-NP/MnO_2 as a function of the current density. (d) Cycle performance of Ag-NW/PEDOT:PSS-NP/MnO_2 at a scan rate of 100 mV s^{-1}.

considerably. Fig. S4 of ESI shows that the curve of pure Ag-NW is close to a line, indicating that the contribution of pure Ag-NW is insignificant. The total area of CV of Ag-NW/PEDOT:PSS-NP is much larger than that of pure PEDOT:PSS-NP, revealing that the high conductivity of Ag-NW is responsible for the better electrochemical property (ESI, Fig. S4). CV curves of Ag-NW/PEDOT:PSS-NP/MnO_2 at various scan rates with potential window ranging from 0 to 0.8 V were also performed and presented in Fig. S6. All of the CV curves show quasi-box shape as the scan rate is increased from 5 to 100 mV s^{-1}, reveals the good capacitive behavior of Ag-NW/PEDOT:PSS-NP/MnO_2.

To study the charge storage capacity of our electrodes, we performed galvanostatic charge/discharge (GCD) measurements. GCD curves of Ag-NW/PEDOT:PSS-NP/MnO_2 were carried out at different current densities with potential windows ranging from 0 to 0.8V and is presented in Fig. 4b. An excellent symmetric behavior is observed in these GCD curves, revealing good electrochemical capacitive characteristics and fast reversible redox reactions. Figure 4c shows the specific capacitance at different current densities. The specific capacitance decreased as the current density is increased. This is due to the rate of redox reaction will be slower when a higher current density is applied.[40]In this case, an electrode might not be fully charged or discharged within one cycle. Hence, a lower current density is preferred in GCD experiment. The highest specific capacitance of the Ag-NW/PEDOT:PSS-NP/MnO_2 is recorded to be 862 F g^{-1} (based on the mass of MnO_2) at a current density of 2.5 A g^{-1}. The present value is higher than the values of MnO_2 based materials such as MnO_2-carbon nanocomposites (145 F g^{-1} at 1 A g^{-1}),[41] MnO_2-carbon nanotube (CNT) nanocomposites (195 F g^{-1} at 1 A g^{-1}),[42] and MnO_2-graphene composites (850 F g^{-1} at 0.25 A g^{-1}).[43] In addition, the present value is also higher than other pseudo-capacitive materials such as $SnSe_2$,[44] SnSe,[44] CoS_2,[45] GeS_2,[46] Mn_3O_4,[47] etc. These results demonstrate that our electrode shows superior characteristics compared to the state-of-the-art materials and can be very promising for SC electrodes. The loading mass of MnO_2 is controllable by varying the electrodeposition time (SI, Figure S7). Higher loading mass of MnO_2 can be readily reached by extending the electrodeposition time. For example, a mass of 0.64 mg cm^{-2} can be easily reached by extending the electrodeposition time to 48 min, and its specific capacitance still remained 241 F g^{-1} at a current density of 2.5 A g^{-1}. The long-term cyclicity of Ag-NW/PEDOT:PSS-NP/MnO_2 was measured using a CV process at a scan rate of 100 mV s^{-1} (Fig. 4d). The capacitance retention is still 87.6% of its initial capacitance after 4000 cycles, revealing its good cycling stability.

Investigation of the bend property of flexible SC is necessary considering its huge potential market in applications such as roll-up display devices, smart sensors, transparent radio frequency identifications, e-papers and flexible wearable electronics.[48-50] Flexible SC were fabricated by sandwiching a porous separator (pre-dipped into Na_2SO_4 aqueous electrolyte) between two identical Ag-NW/PEDOT:PSS-NP/MnO_2 electrodes (Fig. 5a). Here, we carried out bend test of our device under different bend angles ranging from 0 to 180

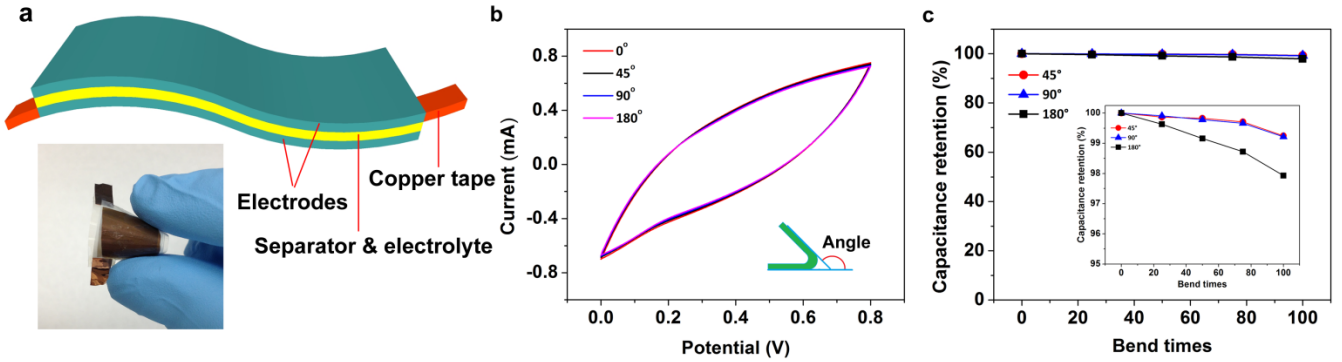

Fig. 5. (a) A schematic diagram of a flexible and sandwich structured SC. Inset: Digital photographs of a flexible SC. (b) CV curves of the SC at different bend angles (0-180°). (c) Capacitance retention as a function of bend times at different bend angles (45-180°). The inset is the enlarged image from capacitance retention 95% to 100 %.

degree. The CV curves of the SC did not change significantly under different bend angles (Fig. 5b), indicating an excellent mechanical property of our device. We also performed a bend test in which the SCs were repeatedly bended at various angles (0 to 180° for 0-100 times) and the results were shown in Fig. 5c. All the SCs exhibited high capacitance retention after 100 bends, even at 180° bend angle. About 98% capacitance retention even after 100 bends at 180°, demonstrates the remarkable flexibility of our SCs.

Gogotsi and Simon had proposed that specific capacitance based on gravimetric unit is nearly irrelevant compared to volumetric unit especially for SC devices built by thin film electrodes, because the weight of active material coated onto a thin film is negligible.[51] Considering this proposal, the specific capacitance of our devices was calculated in terms of volumetric specific capacitance. GCD curves of SC devices at various current densities were shown in Fig. S8. At current density of 0.1 A cm^{-3}, the volumetric specific capacitance of the SC is calculated to be 4.64 F cm^{-3}(volume is based on the whole device), which is substantially larger than the values obtained from recent reports of SCs such as graphene SC 0.4 F cm^{-3},[52] H-TiO_2@MnO_2//H-TiO_2@C SC 0.9 F cm^{-3},[53] VN SC 1.6 F cm^{-3},[54] and Co_9S_8//Co_3O_4@RuO_2 SC 3.5 F cm^{-3}.[55] Such superior performance of Ag-NW/PEDOT:PSS-NP/MnO_2 SC can be attributed to the following factors: (1) highly conductive current collector (Ag-NW/PEDOT:PSS) enables efficient and fast electron transport; (2) nanostructured design provides more electrochemically active sites for redox reactions; (3) direct contact between active material and current collector without a binder enables a low interfacial resistance.

Ragone plot (power density vs energy density) is an important tool to compare the performance of SCs. Fig. 6a shows the Ragone plot of the SC device assembled in this manuscript and some other recent reports for comparison.[52] Our device can exhibit energy density up to 4.06×10^{-4} Wh cm^{-3}, which is comparable to that of lithium thin film battery, 10 times higher than that of graphene SC, and three-orders of magnitude larger than that of aluminum electrolytic capacitor. Moreover, our device can deliver a power density up to 3.69×10^{-1} W cm^{-3}, which is more than 10 times higher than that of lithium thin film battery and comparable to graphene supercapacitor.[52] Furthermore, we assembled two supercapacitors in series and found that the device could power a light-emitting diode (LED) well for about 20 min after charging at 1 mA for 30 s (Fig. 6b). This result reveals the potential of the fabricated flexible supercapacitor device in energy storage.

4. Conclusions

In summary, this study reports a simple, fast, easily reproducible, and cost-effective approach to fabricate novel Ag-

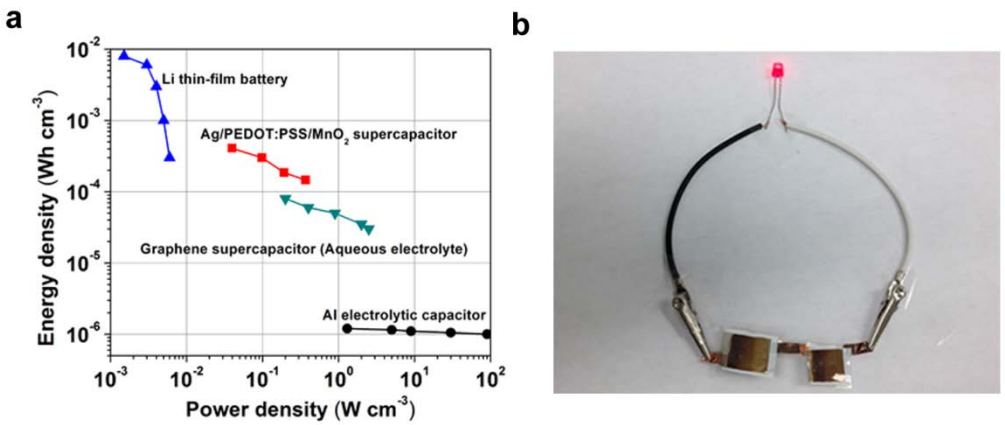

Fig. 6. (a) Ragone plot of Ag-NW/PEDOT:PSS-NP/MnO2 SC compared with graphene SC, aluminum electrolytic capacitor, and lithium thin-film battery.[52] (b) Light-emitting diode (LED) lighting demonstration, with the diode driven by two supercapacitors in series.

NW/PEDOT:PSS-NP/MnO_2 hybrid structure for high performance flexible SCs. In this device design, Ag-NW not only improves the electrical conductivity but also enhances the mechanical stability; PEDOT:PSS-NP provides large surface area for depositing MnO_2 and enables fast and reversible redox reactions; MnO_2 considerably improves the specific capacitance. Ag-NW/PEDOT:PSS-NP/MnO_2 shows remarkable enhancements in specific capacitance, excellent charge/discharge ability, good cycle stability, exceptional bendability, and high energy density. All wet processing method of fabrication and high flexibility and bendability along with excellent performances are some of the promising features of this SC for future energy storage systems.

Acknowledgements

J.T acknowledges NSF EAGER (ECCS 1247838) funding for the completion of this work. The authors thank Materials Characterization Facility (MCF), University of Central Florida for the nanostructure characterization and University of California, Santa Barbara (UCSB) for mold fabrication.

Notes and references

NanoScience Technology Center & Department of Material Science and Engineering & CREOL, College of Optics and Photonics, University of Central Florida, Florida 32826, United States. E-mail: Jayan.Thomas@ucf.edu; Fax: +1 407 882 2819; Tel: +1 407 882 0196

† Electronic Supplementary Information (ESI) available: Capacitive equations, AFM image, CV and GCD curves. See DOI: 10.1039/c000000x/

1. P. Simon and Y. Gogotsi, *Nat. Mater.*, 2008, **7**, 845-854.
2. J. R. Miller and A. F. Burke, *Electrochem. Soc. Interface*, 2008, **17**, 53-57.
3. J. R. Miller and P. Simon, *Science*, 2008, **321**, 651-652.
4. C. C. Hu, K. H. Chang, M. C. Lin and Y. T. Wu, *Nano Lett.*, 2006, **6**, 2690-2695.
5. G. Zhang, L. Yu, H. E. Hoster and X. W. D. Lou, *Nanoscale*, 2013, **5**, 877-881.
6. C. Yuan, L. Yang, L. Hou, L. Shen, X. Zhang and X. W. D. Lou, *Energy Environ. Sci.*, 2012, **5**, 7883-7887.
7. Y. Huang, Y. Li, Z. Hu, G. Wei, J. Guo and J. Liu, *J. Mater. Chem. A*, 2013, **1**, 9809-9813.
8. J. Jiang, Y. Li, J. Liu, X. Huang, C. Yuan and X. W. D. Lou, *Adv. Mater.*, 2012, **24**, 5166-5180.
9. X. Lang, A. Hirata, T. Fujita and M. Chen, *Nat. Nanotechnol.*, 2011, **6**, 232-236.
10. W. Wei, X. Cui, W. Chen and D. G. Ivey, *Chem. Soc. Rev.*, 2011, **40**, 1697-1721.
11. C. Liu, F. Li, L. P. Ma and H. M. Cheng, *Adv. Mater.*, 2010, **22**, E28-E62.
12. A. L. M. Reddy, M. M. Shaijumon, S. R. Gowda and P. M. Ajayan, *J. Phys. Chem. C*, 2009, **114**, 658-663.
13. W. Si, C. Yan, Y. Chen, S. Oswald, L. Han and O. G. Schmidt, *Energy Environ. Sci.*, 2013, **6**, 3218-3223.
14. D. Bélanger, L. Brousse and J. W. Long, *Electrochem. Soc. Interface*, 2008, **17**, 49-52.
15. J. Liu, J. Jiang, C. Cheng, H. Li, J. Zhang, H. Gong and H. J. Fan, *Adv. Mater.*, 2011, **23**, 2076-2081.
16. J. Yan, E. Khoo, A. Sumboja and P. S. Lee, *ACS Nano*, 2010, **4**, 4247-4255.
17. K. Xu, W. Li, Q. Liu, B. Li, X. Liu, L. An, Z. Chen, R. Zou and J. Hu, *J. Mater. Chem. A*, 2014, **2**, 4795-4802.
18. Z. Yu and J. Thomas, *Adv. Mater.*, 2014, DOI: 10.1002/adma.201400440.
19. J. H. Kim, K. H. Lee, L. J. Overzet and G. S. Lee, *Nano Lett.*, 2011, **11**, 2611-2617.
20. H. Zhang, G. Cao, Z. Wang, Y. Yang, Z. Shi and Z. Gu, *Nano Lett.*, 2008, **8**, 2664-2668.
21. A. L. M. Reddy, M. M. Shaijumon, S. R. Gowda and P. M. Ajayan, *Nano Lett.*, 2009, **9**, 1002-1006.
22. R. Zhou, C. Meng, F. Zhu, Q. Li, C. Liu, S. Fan and K. Jiang, *Nanotechnology*, 2010, **21**, 345701.
23. Y. C. Chen, Y. K. Hsu, Y. G. Lin, Y. K. Lin, Y. Y. Horng, L. C. Chen and K. H. Chen, *Electrochim. Acta*, 2011, **56**, 7124-7130.
24. L. Hu, W. Chen, X. Xie, N. Liu, Y. Yang, H. Wu, Y. Yao, M. Pasta, H. N. Alshareef and Y. Cui, *ACS Nano*, 2011, **5**, 8904-8913.
25. P. Yang, Y. Li, Z. Lin, Y. Ding, S. Yue, C. P. Wong, X. Cai, S. Tan and W. Mai, *J. Mater. Chem. A*, 2014, **2**, 595-599.
26. R. Liu and S. B. Lee, *J. Am. Chem. Soc.*, 2008, **130**, 2942-2943.
27. J. Duay, E. Gillette, R. Liu and S. B. Lee, *Phys. Chem. Chem. Phys.*, 2012, **14**, 3329-3337.
28. Z. Yu, B. Duong, D. Abbit and J. Thomas, *Adv. Mater.*, 2013, **25**, 3302-3306.
29. B. Duong, P. Gangopadhyay, J. Brent, S. Seraphin, R. O. Loutfy, N. Peyghambarian and J. Thomas, *Acs Appl. Mater. Interfaces*, 2013, **5**, 3894-3899.
30. B. Duong, Z. Yu, P. Gangopadhyay, S. Seraphin, N. Peyghambarian and J. Thomas, *Adv. Mater. Interfaces*, 2014, **1**, 1300014.
31. A. A. Khosroabadi, P. Gangopadhyay, B. Duong, J. Thomas, A. K. Sigdel, J. J. Berry, T. Gennett, N. Peyghambarian and R. A. Norwood, *Phys. Status Solidi A*, 2013, **210**, 831-838.
32. T. Stöcker, A. Köhler and R. Moos, *J. Polym. Sci., Part B: Polym. Phys.*, 2012, **50**, 976-983.
33. L. Groenendaal, F. Jonas, D. Freitag, H. Pielartzik and J. R. Reynolds, *Adv. Mater.*, 2000, **12**, 481-494.
34. H. D. Nguyen, J. M. Ko, H. J. Kim, S. K. Kim, S. H. Cho, J. D. Nam and J. Y. Lee, *J. Nanosci. Nanotechnol.*, 2008, **8**, 4718-4721.
35. C. Granqvist and A. Hultåker, *Thin Solid Films*, 2002, **411**, 1-5.
36. J. Di, D. Hu, H. Chen, Z. Yong, M. Chen, Z. Feng, Y. Zhu and Q. Li, *ACS Nano*, 2012, **6**, 5457-5464.
37. F. Xu and Y. Zhu, *Adv. Mater.*, 2012, **24**, 5117-5112.
38. C. Zhou, H. Wang, F. Peng, J. Liang, H. Yu and J. Yang, *Langmuir*, 2009, **25**, 7711-7717.
39. Y. Ding, Y. Wang, L. Su, H. Zhang and Y. Lei, *J. Mater. Chem.*, 2010, **20**, 9918-9926.
40. T. Morishita, Y. Soneda, H. Hatori and M. Inagaki, *Electrochim. Acta*, 2007, **52**, 2478-2484.
41. Z. Lei, J. Zhang and X. Zhao, *J. Mater. Chem.*, 2012, **22**, 153-160.
42. J.-H. Kim, K. H. Lee, L. J. Overzet and G. S. Lee, *Nano Lett.*, 2011, **11**, 2611-2617.

43. X. Zhao, L. Zhang, S. Murali, M. D. Stoller, Q. Zhang, Y. Zhu and R. S. Ruoff, *ACS Nano*, 2012, **6**, 5404-5412.
44. C. Zhang, H. Yin, M. Han, Z. Dai, H. Pang, Y. Zheng, Y.-Q. Lan, J. Bao and J. Zhu, *ACS Nano*, 2014, DOI: 10.1021/nn5004315.
45. B. Wang, J. Park, D. Su, C. Wang, H. Ahn and G. Wang, *J. Mater. Chem.*, 2012, **22**, 15750-15756.
46. X. Wang, B. Liu, Q. Wang, W. Song, X. Hou, D. Chen, Y. b. Cheng and G. Shen, *Adv. Mater.*, 2013, **25**, 1479-1486.
47. J. W. Lee, A. S. Hall, J.-D. Kim and T. E. Mallouk, *Chem. Mater.*, 2012, **24**, 1158-1164.
48. S. Park, G. Wang, B. Cho, Y. Kim, S. Song, Y. Ji, M.-H. Yoon and T. Lee, *Nat. Nanotechnol.*, 2012, **7**, 438-442.
49. M. F. El-Kady and R. B. Kaner, *Nat. Commun.*, 2013, **4**, 1475-1483.
50. J. Bae, M. K. Song, Y. J. Park, J. M. Kim, M. Liu and Z. L. Wang, *Angew. Chem. Int. Ed.*, 2011, **50**, 1683-1687.
51. Y. Gogotsi and P. Simon, *Science*, 2011, **334**, 917-918.
52. M. F. El-Kady, V. Strong, S. Dubin and R. B. Kaner, *Science*, 2012, **335**, 1326-1330.
53. X. Lu, M. Yu, G. Wang, T. Zhai, S. Xie, Y. Ling, Y. Tong and Y. Li, *Adv. Mater.*, 2013, **25**, 267-272.
54. X. Lu, M.-H. Yu, T. Zhai, G. Wang, S. Xie, T. Lu, C. Liang, Y.-X. Tong and Y. Li, *Nano Lett.*, 2013, **13**, 2628-2633.
55. J. Xu, Q. Wang, X. Wang, Q. Xiang, B. Liang, D. Chen and G. Shen, *ACS Nano*, 2013, **7**, 5453-5462.

Table of contents entry

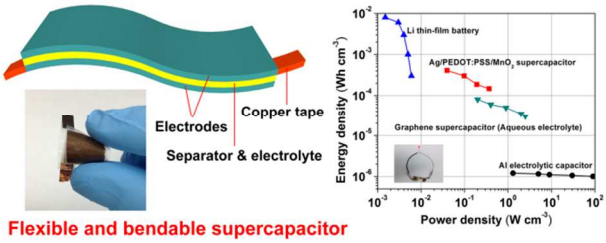

We demonstrate the design and fabrication of a Ag/PEDOT:PSS/MnO_2 layer by layer structure for high performance flexible supercapacitors.